Supplemental Materials

Wrapping up Hydrophobic Hydration – Locality Matters

Authors

V. Conti Nibali,[1†] S. Pezzotti,[2†] F. Sebastiani,[1†] D. R. Galimberti,[2] G. Schwaab,[1] M. Heyden,[3*] M.-P. Gaigeot,[2*] M. Havenith[1*]

Affiliations

[1]Department of Physical Chemistry II, Ruhr University Bochum, Bochum, Germany.

[2] LAMBE CNRS UMR8587, Université d'Evry val d'Essonne & Université Paris-Saclay, Evry, France.

[3] School of Molecular Sciences, Arizona State University, Tempe, AZ, USA.

† These authors contributed equally to this work: V. Conti Nibali, S. Pezzotti, F. Sebastiani

*email: mheyden1@asu.edu; mgaigeot@univ-evry.fr; martina.havenith@rub.de.

CLASSICAL MOLECULAR DYNAMICS SIMULATIONS

Classical molecular dynamics simulations of *tert*-butanol (2-methyl-2-propanol) solvated in water were carried out with the Gromacs 4.6.1 software package[1]. The OPLS all-atom force field[2] was used to describe the solute molecule, while the TIP4P-2005 model was used for water[3]. The coordinates of the solute molecule were optimized with respect to the internal energy prior to placing it in the center of a cubic box containing 881 water molecules with an initial edge length of ~40 Å. In the following simulations, the coordinates of the solute atoms were kept fixed to allow for a high-resolution analysis of hydration water properties in its environment (see below). In all simulations, long range electrostatics were treated with the particle mesh Ewald algorithm on a 1.2 Å spatial grid with a fourth order interpolation[4,5].

Short-range electrostatic and Lennard-Jones forces were shifted to zero between 9.0 and 10.0 Å. Long-range dispersion corrections were applied for the energy and pressure. Neighbour lists were updated every 10 femtoseconds (fs) (equilibration) or 8 fs (production) with a 13.0 Å distance cutoff. The time step for integration was set to 1 fs (for both equilibration and production). The SETTLE algorithm[6] was used to constrain the intramolecular degrees of freedom of water molecules.

The system was equilibrated for 1 nanosecond (ns) in the isobaric-isothermal (NPT) ensemble at a pressure of 1 bar and the target temperature (273 K, 283 K, 293 K, 303 K, 313 K) using temperature coupling via a stochastic velocity rescaling thermostat[7] and a Berendsen weak-coupling barostat[8] with a time constant of 1.0 picosecond (ps). This was followed by a 100 ns production run in the canonical (NVT) ensemble at the same temperature as the equilibration using a Nose-Hoover thermostat[9,10] with a time constant of 5.0 ps. During the production run, coordinates and velocities were saved every 8 fs for subsequent analysis.

SPATIALLY RESOLVED TETRAHEDRAL ORIENTATIONAL ORDER PARAMETER

We quantified the tetrahedral character of local molecular environments in our simulation using the orientational order parameter introduced by Errington and Debenedetti[11], which describes the angular distribution of the four nearest neighbours of a molecule.

$$q = 1 - \frac{3}{8}\sum_{j=1}^{3}\sum_{k=j+1}^{4}\left(\cos\psi_{jk} + \frac{1}{3}\right)^2 \qquad (1)$$

Here, ψ_{jk} describes the angle between vectors connecting a central molecule to its j'th and k'th nearest neighbors. This order parameter is constructed to provide 1 for perfectly tetrahedral environments and 0 for an ideal gas (negative values are possible). We applied this measure to water oxygen atoms in the hydration shell of the *tert*-butanol solute, including the oxygen atom of the alcohol group as a potentially coordinating site. The analysis was performed on a three-dimensional cubic grid centered on the immobilized solute molecule to spatially resolve the local

tetrahedral order, $q_{local}(\boldsymbol{r})$, of water molecules in the solute hydration shell. The grid contains 32 x 32 x 32 volume elements (voxels) with a grid constant of 0.5 Å. Water molecules analyzed for a given time frame of the trajectory were assigned to a voxel based on their center of mass position.

We focused our analysis on variations of the time-averaged local tetrahedral order from the bulk water average, which was obtained from voxels separated by 9 Å or more from the closest solute atom. The bulk water average q is 0.704±0.002 (273 K), 0.691±0.003 (283 K), 0.674±0.002 (293 K), 0.661±0.002 (303 K), 0.649±0.002 (313 K). To highlight tetrahedral and non-tetrahedral water, we selected two categories of voxels, q_{HIGH} and q_{LOW}, that have, respectively, a positive and a negative deviation of $q_{local}(\boldsymbol{r})$ from the bulk water average q_{bulk}. Both are defined by a minimum deviation of $q_{local}(\boldsymbol{r})$ from q_{bulk} at a given temperature by more than 2.5 standard deviations σ_q of bulk water local order parameters.

Figure S1 shows the spatial distribution of voxels with a positive and negative deviation of $q_{local}(\boldsymbol{r})$ from the bulk water average q_{bulk} for various temperatures. For clarity, voxels are shown for which a minimum average local number density of 20% of the bulk water was observed at the given temperature.

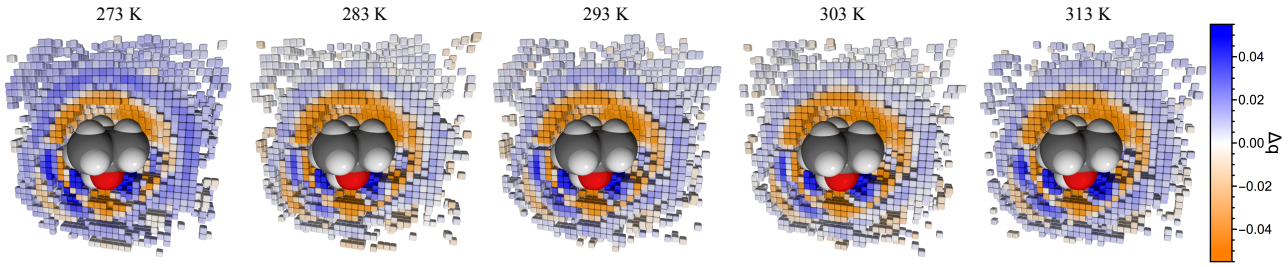

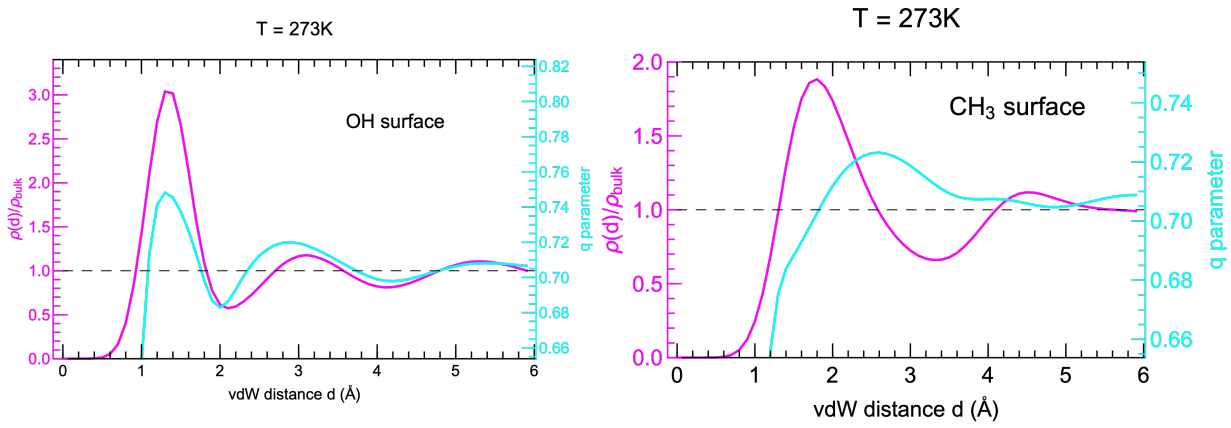

Figure S1: 3D water q maps around tBuOH (273 – 313 K). Top: *Illustration of the tert-butanol molecule and its solvation environment in the investigated temperature range. Voxels of the analysis grid are colored based on the difference* $\Delta q(\boldsymbol{r}) = q_{local}(\boldsymbol{r}) - q_{bulk}$. *Orange (blue) voxels describe a less (more) tetrahedral environment with respect to the bulk value and more intense colors describe larger variations. Only voxels with a positive x–coordinate are shown for clarity.* **Bottom.** *Radially resolved q parameter (cyan, right y-axes) around OH (left) and* CH_3 *(right) groups are compared to the water center of mass density profiles (magenta, left y-axes) at T=273 K. The dashed line indicates the bulk value. Distances are calculated relative to the vdW-surface of the respective functional group.*

The number of water molecules contributing to the q_{HIGH} and q_{LOW} categories is temperature-dependent. At 273 K, the average number of water molecules contributing to the q_{HIGH} category is 38.8 (obtained from integrating the average local number densities in the corresponding voxels), while 8.8 water molecules fall into the q_{LOW} category. At 313 K, the number of water molecules in the q_{HIGH} category decreases to 25.7, while the number of water molecules in the q_{LOW} category increases to 11.7.

Additionally, we have analyzed the radial profiles of the q parameter in the environment of the different chemical groups of the *tert*-butanol molecule, i.e. the OH and the CH_3 groups. In Figure S1 (bottom) the q profile for each group is compared to the number density profile of water molecule centers of mass in the hydration shell of the group.

SPATIALLY RESOLVED SOLVATION ENTROPY

To spatially resolve local molecular entropies of water in the hydration shell of the *tert*-butanol molecule, we adopted the 3D-2PT approach by Persson *et al.*[12]. This approach is an extension of the two-phase thermodynamics (2PT) method[13] to allow for a spatially resolved analysis on a grid in analogy to our analysis of the local tetrahedral order parameter described above. Local velocity autocorrelation functions are computed for delay times up to 1.6 picoseconds (ps) directly from the molecular dynamics trajectories. Translational and rotational degrees of freedom of the rigid water molecules are treated separately. The Fourier transform of the correlation functions describes the local vibrational density of states (DOS), which is then used to calculate the local entropy per molecule via the 2PT expressions for rigid molecules[13]. The bulk water entropy per molecule, S_{bulk}, is obtained as an average for voxels far from the solute, in accordance to the definition for q_{bulk} in the previous section. In Figure S2, we report the spatially resolved changes of the molecular entropy

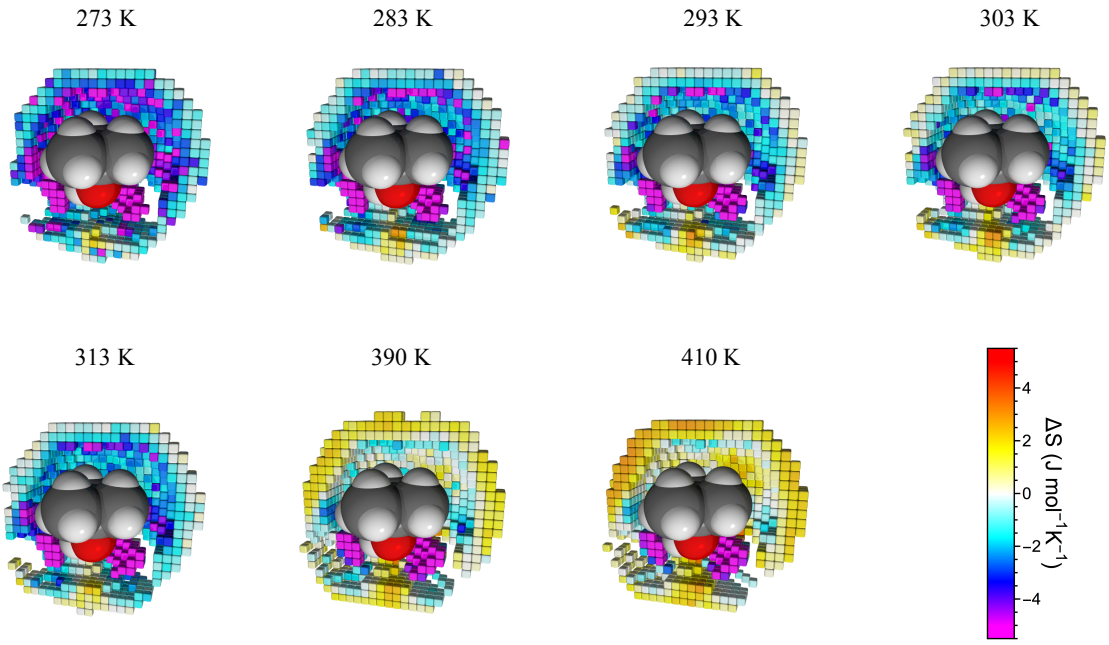

of water relative to the bulk in the environment of *tert*-butanol.

Figure S2. 3D water entropy maps around tBuOH (273 – 410 K). *Illustration of the tert-butanol solute and its solvation environment in the investigated temperature range. Voxels of the analysis grid are colored based on local deviations of the molecular entropy from the bulk value,* $\Delta S(\mathbf{r})=S(\mathbf{r})-S_{bulk}$*. Distinct from Figure S1, we focus here on favorable hydration sites by showing voxels with a local number density equal to or larger than that of bulk water and within a distance of 5 Å from the closest atom of the solute. Further, only voxels with a positive x–coordinate are shown for clarity.*

EXPERIMENTAL METHODS AND DATA ANALYSIS

Materials and methods

Tert-butanol (tBuOH) with a nominal purity higher than 99% was purchased from VWR International (Germany), and dissolved in HPLC water. Temperature-dependent, low frequency spectra of *tert*-butanol aqueous solution at 0.5 M were recorded at five different temperatures (274 K, 283 K, 293 K, 303 K, and 313 K) in the frequency range between 50 and 600 cm^{-1}. Concentration-dependent, low frequency spectra of *tert*-butanol aqueous solutions at 0.2, 0.5, 1, 2, 3, 4 and 5 M were measured in the frequency range from 50 to 450 cm^{-1} at room temperature.

We used a Bruker Vertex 80v FTIR spectrometer equipped with a liquid helium cooled silicon bolometer from Infrared Laboratories as a detector. The sample solutions were placed in a temperature controlled liquid transmission cell from Harrick Scientific Products (USA) with two 0.5 mm-thick polycristalline diamond windows supplied by Diamond Materials (Germany) and Kapton spacers of about 15 and 25 μm thickness for temperature- and concentration-dependent measurements, respectively. The exact sample layer thickness was determined by recording etalons of the empty cell before each series of measurements. For each single spectrum, 128 scans were averaged with a resolution of 2 cm^{-1}. The spectra were smoothened with a 2 cm^{-1} wide (5 points) moving average. During each series of measurements, the sample compartment was continuously purged with technical grade dry nitrogen to minimize air humidity.

Data analysis

The data analysis is carried out in the same way as described in detail in Refs.[14,15], Here, we just summarize the main steps. In Figure S3 (top-left), we show the absorption coefficient of aqueous *tert*-butanol solutions as a function of concentrations at 300 K. Using Lambert-Beer's Law, the frequency-, concentration- and temperature-dependent absorption coefficient of the solution ($\alpha_{\mathrm{solution}}(\nu, c_s, T)$) is expressed as:

$$\alpha_{\mathrm{solution}}(\nu, c_s, T) = \frac{1}{d} \ln\left(\frac{I_{\mathrm{water}}(\nu,T)}{I_{\mathrm{solution}}(\nu,c_s,T)}\right) + \alpha_{\mathrm{water}}(\nu, T) \qquad (2)$$

where d is the sample thickness, $I_{\mathrm{water}}(\nu, T)$ and $I_{\mathrm{solution}}(\nu, c_s, T)$ are the transmitted intensities of the water reference and the sample at temperature T and concentration c_s, respectively. $\alpha_{\mathrm{water}}(\nu, T)$ is obtained from a fit of the absorption spectrum of water at a given temperature T. Taking water as a reference (i.e. subtracting the bulk water signal) helped to eliminate spectral features due to reflections at the cell windows of the sample cell. The residual absorption due to residual air in the absorption path was corrected by taking into account a scaled spectrum of water vapor.

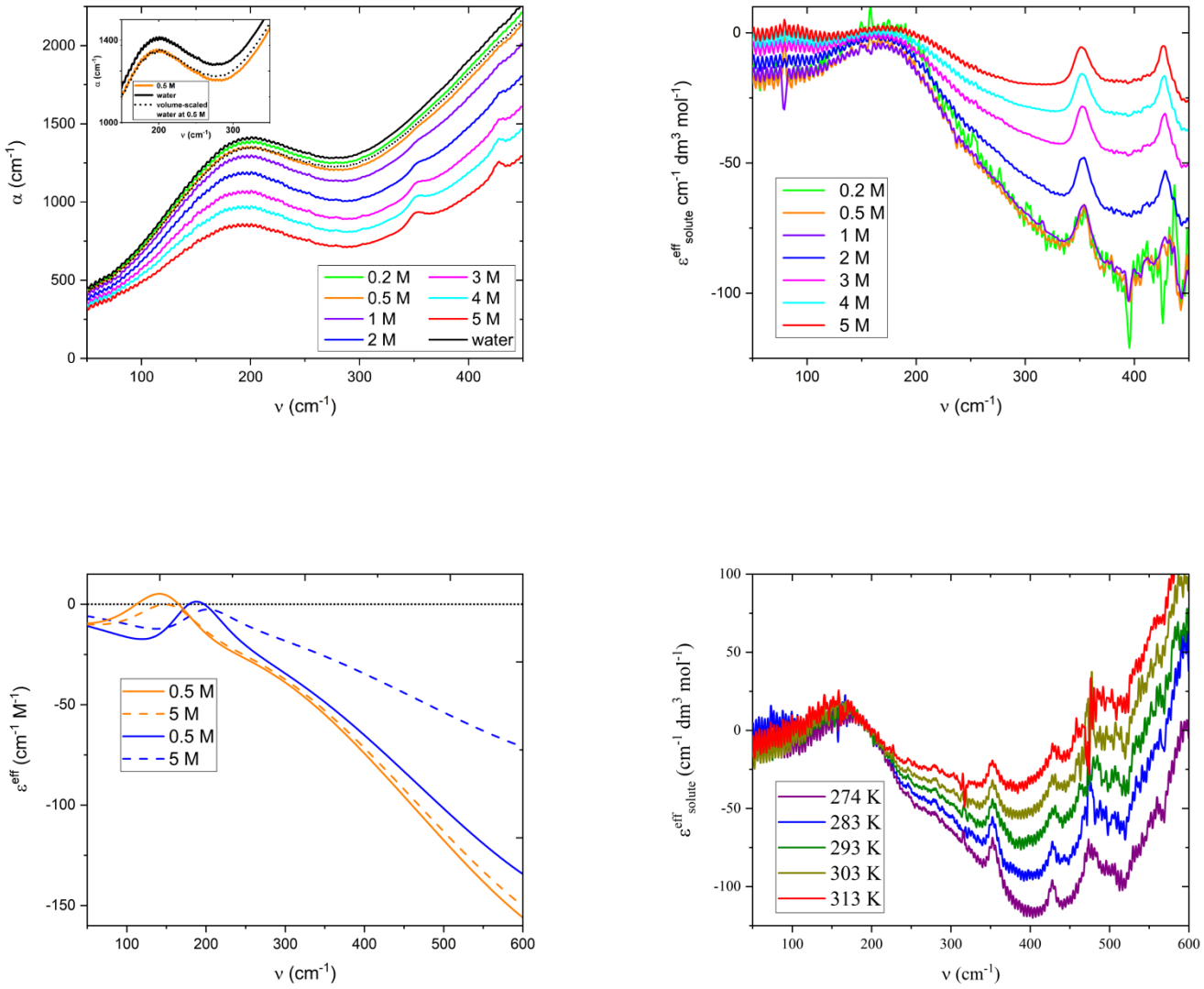

Figure S3: Absorption and extinction spectra of tBuOH at different concentrations and temperatures. ***(top-left)*** *Absorption coefficient of tBuOH solutions at different concentrations at 293 K ($\alpha_{solution}$). Bulk water absorption is displayed for comparison (α_{water}). Inset: Absorption coefficient of bulk water and tBuOH solution at 0.5 M. The dotted line represents the partial water absorption, as obtained by taking into account the excluded volume of the solute at 0.5 M.* ***(top-right)*** *Effective molar extinction spectra of tBuOH solutions at different concentrations at 293 K.* ***(bottom-left)*** *Contribution of the two hydration water bands at 164 and 195 cm^{-1}, shown in orange and blue, respectively, to the total experimental difference spectrum for 0.5 M (solid lines) and 5 M (dashed lines) solutions of tBuOH at 293 K. We subtracted the bulk water contribution due to solvent displacement by the solute (see text). The experimental error is on the order of 5%.* ***(bottom-right)*** *Effective molar extinction spectra of the tBuOH solution at 0.5 M as a function of temperature.*

To take into account the replacement of water molecules by the presence of the hydrated solute,[14,15] the effective absorption coefficient of the solvated solute at a specific concentration (c_s) and temperature (T) (or absorption difference spectrum) can be deduced from the following equation:

$$\alpha_{\mathrm{difference}}(\nu, c_s, T) = \alpha_{\mathrm{solution}}(\nu, c_s, T) - \frac{c_w}{c_{w,b}}\alpha_{\mathrm{water}}(\nu, T), \qquad (3)$$

where c_w and $c_{w,b}$ are the water concentrations in the solution and in bulk water at the same temperature, respectively. The dotted line in the Inset of Figure S3 (top-left) represents the partial water absorption, as obtained by taking into account the excluded volume by the solute of a 0.5 M solution. Thus, the effective molar extinction coefficient of the solvated solute is:

$$\varepsilon^{\mathrm{eff}}_{\mathrm{solute}}(\nu, T) = \frac{\alpha_{\mathrm{difference}}(\nu, c_s, T)}{c_s} \qquad (4)$$

The results for $\varepsilon^{\mathrm{eff}}_{\mathrm{solute}}(\nu, T)$ at different concentrations at room temperature and for the 0.5 M *tert*-butanol solution as a function of temperature are shown in Figure S3 (top-right and bottom right).

As routinely done in THz-Far Infrared absorption data analysis (see for example Refs.14 and 15), the experimental molar extinction spectra from 50 to 360 cm^{-1} were fitted using a superposition of a negative contribution ($-n_{\mathrm{hydr}}\varepsilon_{\mathrm{water}}$, being n_{hydr} the effective number of hydration water molecules per solute) due to bulk water replacement by hydration water and a sum of damped harmonic oscillator functions for the hydration water modes:

$$\varepsilon_{\mathrm{DHO}}(\nu) = \frac{a \cdot w^2 \cdot \nu^2}{4\pi^3\left((\nu_d^2 + \frac{w^2}{4\pi^2} - \nu^2)^2 + \frac{w^2}{\pi^2}\nu^2\right)} \qquad (5)$$

with a, w, and $\tilde{\nu}_d$ describing the amplitude, the width and the perturbed center frequency of the mode, respectively. The unperturbed center frequency can then be deduced accordingly:

$$\nu_0 = \sqrt{\nu_d^2 + \frac{w^2}{4\pi^2}} \qquad (6)$$

Concentration-dependent analysis

It was shown[14] that the main contribution of hydration water for a number of solvated alcohols (MeOH, EtOH, PrOH, BuOH, PeOH, tBuOH) between 274 K and 310 K, in the low frequency

spectra (from 50 to 350 cm^{-1}) can be decomposed into two bands with unperturbed center frequencies of 164 cm^{-1} and 195 cm^{-1}, respectively. While the amplitude of each of these two bands is temperature- and solute-dependent, the center frequency and the line width could be kept constant in the final global fit irrespective of the choice of solute and temperature. The same analysis was performed on the effective molar extinction coefficients of tBuOH solutions at different concentrations (0.2, 0.5, 1, 2, 3, 4 and 5 M) at room temperature. For further analysis, the line widths of the two hydration water bands were fixed to the same value as in the temperature-dependent measurements in the fitting procedure. The fit results are shown in Figure S3(bottom-left) for the 0.5 and 5 M solutions and are listed in Table S1 for all the investigated concentrations.

As reported in Table S1, we observed for each concentration a hydration water band at 164 cm^{-1} within error bars. We found also, irrespective of concentration, a second band close to 195 cm^{-1}. However, for the latter a small blue shift is observed at higher concentrations ≥ 3M. It should be noted that at concentrations above 2 M, the hydration shell can be shared by two solutes, as this is the onset of aggregation.[16-19] On the contrary, in Raman-MCR and polarization-resolved femtosecond infrared studies of the mixture, it was inferred that the number of aggregates agree with the assumption of a random mixture.[20,21]

As also listed in Table S1, the amplitude of the 195 cm^{-1} mode decreases faster with increasing concentration of the alcohol than the amplitude of the 164 cm^{-1} mode within error bars. In Figure 1 in the Main Text, the intensity fractions of each single band with respect to the total signal is reported, namely $a_\nu/(a_{164} + a_{195})$, where a_ν is the fitted amplitude of the corresponding damped harmonic oscillator with ν=164, 195 cm^{-1}, while the number of water molecules contributing to each hydration bands at 164 cm^{-1} and 195 cm^{-1} is defined as $n_\nu = \frac{a_\nu n_{hydr}}{a_{164}+a_{195}}$ with ν =164 or 195 cm^{-1} (as in Ref.14) and is shown in Fig. S4.

Concentration (M)	ν_{164} (cm^{-1})	a_{164} (cm^{-1} dm^3 mol^{-1})	ν_{195} (cm^{-1})	a_{195} (cm^{-1} dm^3 mol^{-1})
0.2	162 (3)	771(71)	191 (1)	664(70)
0.5	161 (2)	715(53)	190 (1)	611(53)
1	159 (2)	673(40)	190 (1)	609(40)
2	163 (1)	797(85)	193 (2)	478(29)
3	164 (1)	726(71)	196 (2)	396(24)
4	165 (1)	663(70)	198 (2)	344(24)
5	167 (1)	725(70)	200 (2)	293(25)

Table S1. Fit results of the hydration water bands for tBuOH solutions. *Results of the fit of two hydration water bands as a function of concentration. Their center frequencies (ν_{164} and ν_{195}) and their amplitudes (a_{164} and a_{195}) are given with their 2σ errors in brackets.*

For a direct comparison with the ab initio simulations we subtracted the corresponding partial negative contribution of bulk water due to solvent replacement (i.e. $-n_\nu \varepsilon_{water}$, with ν = 164 or 195 cm^{-1}) from each fitted partial contribution of hydration water (i.e. the modes at 164 and 195 cm^{-1}, respectively). This is shown for tBuOH solutions at 0.5 and 5 M in Figure 1 in the Main Text and in Figure S3 (bottom-left panel).

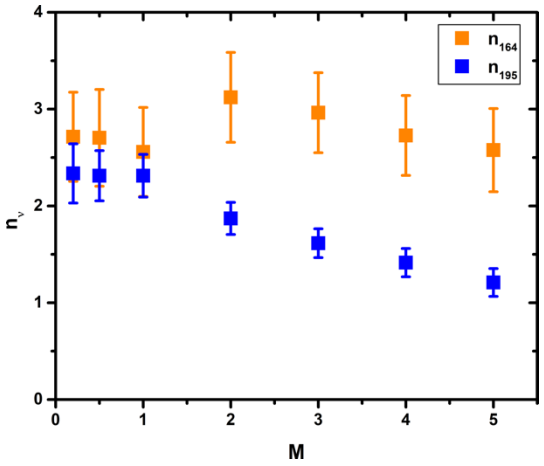

Figure S4. Number of hydration water molecules at different concentrations of tBuOH. *Number of hydration water molecules contributing to the corresponding hydration water bands at 164 cm^{-1} (orange points) and 195 cm^{-1} (blue points) for tBuOH aqueous solutions as increasing concentration at 293 K.*

Temperature-dependent analysis

We found that the temperature dependence of the number of water molecules for each hydration water mode at 164 and 195 cm^{-1} (n_{164} and n_{195} , respectively) can be well approximated by a two-state model[14]

$$n_\nu(T) = \frac{n_\nu(0)}{1+e^{\frac{\Delta H_\nu}{R}(\frac{1}{T}-\frac{1}{T_{\nu,melt}})}} \qquad (7)$$

with ν=164 and 195, and ΔH_ν being the enthalpic energy difference between the involved states, R as universal gas constant. $T_{\nu,melt}$, the melting temperature, i.e. the temperature where both states are equally populated. The results of a fit for the *tert*-butanol solution at 0.5 M are summarized in Table S2[14] and shown in Figure 3 in the Main text.

Each partial hydration water mode contribution probes a distinct water network structure with a distinct, characteristic ∂H^2. Thus, a mode specific heat capacity (C_p), which differs from that of bulk water, is assigned to each of the bands at 164 and 195 cm^{-1} (i.e. C_p^{164} and C_p^{195}).

$n_{164}(0)$	ΔH_{164} (kJ/mol)	$T_{164,ref}$ (K)	$n_{195}(0)$	ΔH_{195} (kJ/mol)	$T_{195,melt}$ (K)
3.65(9)	63(10)	329(4)	12.4(26)	40(3)	271(6)

	ΔC_p^{164} (kJ/mol/K)	ΔC_p^{195} (kJ/mol/K)	ΔC_p400 (kJ/mol/K)	ΔS400 (kJ/mol/K)	ΔH400 (kJ/mol)
tBuOH			111(6)	-32(1.0)	-1.3(0.4)
Hydration	35.5(2.3)	8.2(8)			

Table S2: Thermodynamic parameters and fit results for tBuOH solutions. (upper part) *Results of a global two component fit of the observed hydration numbers as a function of temperature for tert-butanol.* ***(lower part)*** *Results of a fit of tert-butanol solutions using $n_{164}(T)$ and $n_{195}(T)$ as inputs. The reference temperature is 400 K. ΔC_p^{164}, ΔC_p^{195} are the difference in heat capacity compared to bulk water.*

In Ref.[14] we now made the following ansatz for the mixing heat capacity with respect to a reference temperature (T_{ref}):

$$\Delta C_p(T, T_{ref}) = n_{164}(T)\left(C_p^{164} - C_p^{w,bulk}\right) + n_{195}(T)\left(C_p^{195} - C_p^{w,bulk}\right) + \Delta C_p^{solute}(T_{ref}). \quad (8)$$

Temperature dependence of ΔC_p are attributed exclusively to changes in $n_{164}(T)$ and $n_{195}(T)$, while $\left(C_p^{164} - C_p^{w,bulk}\right) = \Delta C_p^{164}$ and $\left(C_p^{195} - C_p^{w,bulk}\right) = \Delta C_p^{195}$ are temperature independent. $\Delta C_p^{solute}(T_{ref})$ is a solute-specific parameter which summarizes all solute-specific changes of the heat capacity at a given reference temperature.

Based upon $\Delta C_p(T)$ the temperature dependence of the mixing entropy S (as well as the enthalpy H) was determined:[14]

$$S(T_1) - S(T_0) = \int_{T_0}^{T_1} \frac{\Delta C_p(T)}{T} dT = \Delta C_p^{solute}(T_0) \log\left(\frac{T_1}{T_0}\right) + \Delta S_{164}(T_1) + \Delta S_{195}(T_1) \,. \quad (9)$$

To separate the temperature dependence of the thermodynamic functions related to the observed spectral changes, which are correlated to local hydration changes, from the global solvation changes, we used a reference temperature of 400 K. This is well beyond the highest melting temperature of 330 K for the 164 cm^{-1} band and we calculated any change in thermodynamic parameter with respect to this reference temperature. The results for tert-butanol (tBuOH) are summarized in Table S2 (see also Ref.[14] and references therein).

The spatial resolution of hydration water entropies and local solvation entropy contributions, $\Delta S(\mathbf{r})$, obtained from molecular dynamics simulations via the 3D-2PT analysis can be estimated by integration of the product of $\Delta S(\boldsymbol{r}) = S(\boldsymbol{r}) - S_{bulk}$ and the local number density $n_w(\boldsymbol{r})$ over the analysis grid:

$$\Delta S_{solv} = \int [S(\boldsymbol{r}) - S_{bulk}]\, n_w(\boldsymbol{r}) d\boldsymbol{r} \quad (10)$$

We consider only voxels with a local number density larger than 20% of the bulk density in the integral to ensure statistically converged data and thus ignore low occupation sites, which provide only a negligible contribution to the total solvation entropy in the 3D-2PT description (see Persson *et al.*[12] for further details and the indirect estimation of cavity formation contributions).

Following the analysis of the experimental data, we carried out additional simulations for temperatures of 390 K and 410 K (production simulations in the NVT ensemble and the system size remained approximately constant during preceding, short NPT equilibration simulations) to determine a high temperature reference for $\Delta C_P(T_{ref} = 400\ \mathrm{K})$ via finite differences. This high temperature reference value is assumed to describe a constant baseline for $\Delta C_P(T)$. The remaining temperature-dependence of $\Delta C_P(T)$ at lower temperature is then fully ascribed to structural changes in the hydration shell.

DFT-BASED MOLECULAR DYNAMICS SIMULATIONS

Born-Oppenheimer DFT-based Molecular Dynamics simulations (DFT-MD) have been carried out on a 0.2 M aqueous solution of *tert*-butanol at two temperatures of 290 K and 310 K. The CP2K package[22,23] is employed, the electronic representation consists in the BLYP[24,25] functional including Grimme D2 correction for dispersion,[26,27] GTH pseudopotentials[28] for all atoms, and a combined Plane-Wave (400 Ry density cutoff) and TZV2P gaussian basis sets. The classical Newton's equations of motion for the nuclei are integrated through the Verlet algorithm with a time-step of 0.4 fs. The cubic simulation box (19.734 Å) is composed by a liquid phase made of 256 water molecules solvating one *tert*-butanol molecule, periodically repeated in the 3 directions of space. After an equilibration period of 5 ps (NVE ensemble with possible rescaling of velocities followed by pure NVE ensemble), runs of 50 ps in the NVE ensemble are accumulated, with a final average temperature of 290 K ± 4 K and 310 K ± 5 K respectively for each simulation.

A reference simulation of bulk water has also been run with the same computation set-up and at the same temperature for 50 ps after equilibration. The bulk-water reference simulation consists of 256 water molecules in a cubic box of 19.734 Ang length in each direction. The water density in the simulation is 0.0333 Angstrom^{-3} = 0.996 g/cm^3, coherent with the BLYP-D2 DFT functional applied in the AIMD simulations. For comparison, DFT-MD simulation of the air-water interface already published in Ref.[29], have been continued up to 50 ps to reach the same simulation time as for aqueous *tert*-butanol.

The theoretical IR spectra have been calculated using our previously developed strategy[30] based on the Fourier transform of the correlation function of velocities modulated by Atomic Polar Tensors (APT). This methodology naturally takes into account both the charges and the charge fluxes contributions to the IR intensities (the latter have been shown to be dominant both in the higher and lower frequency domain in the case of H-bonded systems[31,32], while the APT formalism allows a

straightforward decoupling of the IR signal into individual molecule(s)/atom(s) contributions. The IR spectrum is calculated via:

$$I(\omega) = \frac{2\pi\beta}{3cV} \sum_{u=x,y,z} \sum_{m=1}^{3N} \sum_{l=1}^{3N} \int_{-\infty}^{+\infty} dt\, e^{i\omega t} \langle P_{um}(t) v_m(t) P_{ul}(0) v_l(0) \rangle \qquad (11)$$

$\beta = 1/kT$, ω is the frequency of absorbed light, c is the speed of light, V is the volume of the system, $\langle \cdots \rangle$ the equilibrium time correlation function, N is the number of atoms of the system, v_m is the m^{th} element of the $\boldsymbol{v}$ vector that collects the 3N cartesian velocities of the N atoms of the system: $\boldsymbol{v} = [v_{x1}, v_{y1}, v_{z1}, v_{x2}, \ldots v_{zN}]$. $P_{um} = \partial\mu_u/\partial\xi_m$ is the *um* element of the atomic polar tensor, i.e. the first derivative of the u^{th} component (u=x,y,z) of the total dipole moment $\boldsymbol{\mu}$ of the system with respect to the m^{tth} cartesian coordinate ξ_m, $\boldsymbol{\xi} = [x_1, y_1, z_1, x_2, \ldots z_N]$. Eq.11 takes into account all self- and cross-correlation terms, whether intra- or inter-molecular.

By selecting the cartesian coordinates of the atoms belonging to a specific population into the summation in Eq.11, one gets the individual contribution of the selected population to the IR spectrum. As demonstrated in Ref.[30], Eq.11 for IR spectroscopy simultaneously reduces the computational cost from the usual Fourier transform of the dipole moment correlation and accelerates signal convergence, without loss in accuracy. Velocities (v_m) are indeed readily obtained from the DFT-MD trajectories while $\mathbf{P}(t)$ tensors can be parameterized on reference structures.

The present APT parameterization is based on clusters of water molecules, including one target water plus all the water molecules in its first and second solvation shell, randomly extracted from DFT-MD simulations: (1) first solvation shell of the *tert*-butanol immersed in liquid water, (2) bulk liquid water at room temperature and (3) water at the air-water interface. The clusters have been classified considering the number of H-Bonds of the target water molecule (i.e. 1-4) and the nature (i.e. acceptor, donor) of these H-bonds, for a total of 9 classes, leading to 27 (9*3) reference

conformations. A total of 135 clusters (five clusters for each conformation) have been extracted. In these conformations, the APT tensors of the central (target) water molecule in the cluster have been calculated with the Gaussian09 code[33] and the final APT values (used for the spectroscopy calculations) have been obtained by averaging over the 5 clusters extracted for each reference conformation. The APT parameterization has been done in the water molecular frame and one goes from this frame into the laboratory frame in the DFT-MD trajectory with the following equation:

$$\boldsymbol{P}^{\boldsymbol{H_2O}}(t) = \sum_j w_j(t)\boldsymbol{R_j}(ref \rightarrow t)\boldsymbol{P_j^{H_2O,ref}}(ref)\boldsymbol{R_j^T}(ref \rightarrow t) \qquad (12)$$

where j is an index running over the reference structures (two in the present case: 1st shell and bulk), $P_j^{H_2O,ref}$ is the APT tensor for the j^{th} reference structure, w_j is a step function that assigns instantaneously a water molecule to one of the 27 reference conformations described above, and $R_j(ref \rightarrow t)$ is the rotational matrix projecting the molecular frame onto the laboratory frame for each water molecule.

Room temperature (300 K) theoretical THz IR spectrum of bulk liquid water

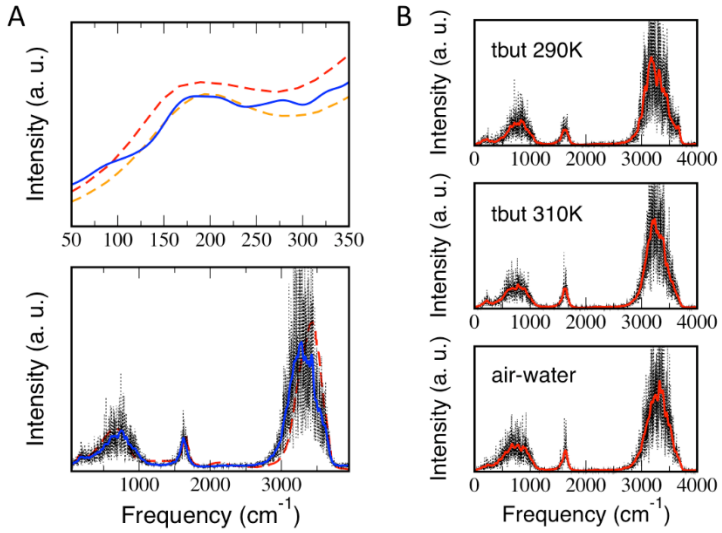

Figure S5: (A) *Theoretical IR spectrum (blue solid lines) calculated using Eq.11 for the reference simulation of bulk liquid. Bottom: 0-4000 cm^{-1} region, compared to experimental spectrum from Ref.[35](red dashed line), top: zoom in the 50-350 cm^{-1} region, compared to experimental spectra from Ref.[35] (red dashed line) and Ref.[14](orange dashed line). The raw data as obtained from DFT-MD calculations are also plotted in black and superimposed with the theoretical spectra obtained with a Gaussian smoothing with 35 cm^{-1}*

(blue solid lines). ***(B)*** *Theoretical IR spectra calculated for the hydration shell of tert-butanol from DFT-MD at temperatures of 290 K (top) and 310 K (middle), as well as for a simulation of the air-water interface at room temperature. The row data are also plotted in black and superimposed with the theoretical spectra obtained with a Gaussian smoothing with 35 cm^{-1} (red).*

The accuracy of the above developed methodology to calculate IR spectra from velocity correlation functions is first tested on the IR spectrum of bulk liquid water in Figure S5 (A).

The whole spectral range calculated water spectrum is in good agreement with experiments[35]. The ratio between the librational, bending and stretching bands obtained from our theoretical spectrum is 4.4:1.0:13.5, in very good agreement with the values of 4.4:1.0:12.9 from experiment[35]. The zoom in the THz region (between 50 and 350 cm^{-1}) allows to appreciate the very good agreement of our calculation also obtained in this region (of main interest for the present work) when compared to experiments in Refs.[14,35].

Theoretical IR THz spectra of 0.2 M aqueous solutions of *tert*-butanol at 290 K and 310 K.

Figure S6-A reports the theoretical difference THz spectra (of water hydrating *tert*-butanol minus bulk water) calculated for each of the HB-wrap and Hydration2bulk populations (see text for their definition). The theoretical spectra calculated for the two interfacial HB populations are compared to the two positive components of the three components fit of the experimentally measured difference spectra of aqueous *tert*-butanol minus bulk water, for the two temperatures of 290 K and 310 K.

The difference spectrum for the HB-wrap/Hydration2bulk population has been calculated as the difference between the signal arising from the HBs of the water molecules within the hydration layer of *tert*-butanol forming the HB-wrap/Hydration2bulk hydrogen bonds minus the signal arising from the bulk water H-Bonds, both normalized by the corresponding number of H-Bonds. As seen in Figure S6-A, this gives rise to two bands in the difference spectrum: one positive band with a maximum at 164 cm^{-1} /195 cm^{-1} for the HB-wrap/Hydration2bulk population (specific of the

hydration layer and not of the bulk, thus the positive intensity), and one negative band with a minimum at 195 cm^{-1} (specific of the bulk and not of the hydration layer, thus the negative intensity).

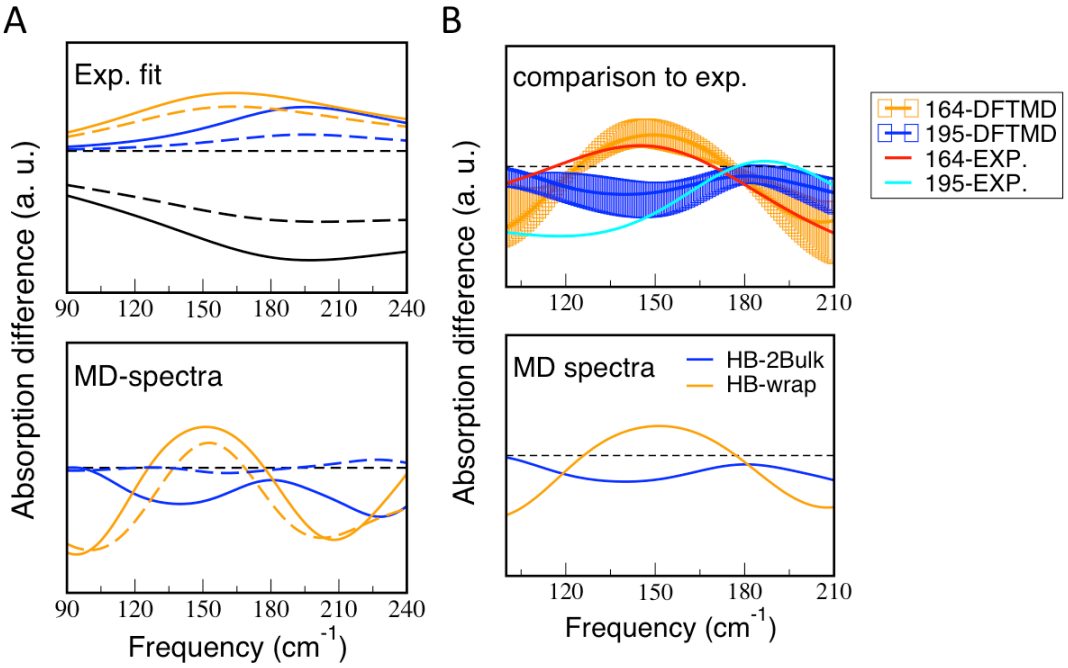

Figure S6: ***(A)*** *Up: Three-components fit of the experimental difference spectra for a 0.5 M aqueous solution of tert-butanol at 290 K (solid line) and 310 K (dashed line), showing the temperature dependence of the two positive components of the fit, related to the HB-wrap (orange) and Hydration2bulk (blue) populations, as well as of the negative component of the fit (black), related to H-Bonds formed by bulk water molecules filling an equivalent volume to the one occupied by the solute and its hydration layer. Bottom: Theoretical difference spectra calculated from DFT- MD for each of the two interfacial H-Bond populations separately, HB-wrap (orange) and Hydration2bulk (blue), at both 290 K (solid line) and 310 K (dashed line).* ***(B)*** *Top: Two hydration water components (red and cyan) of the experimental difference spectrum for a 0.5 M aqueous solution of tert-butanol at 290 K referenced to the absorption of their respective number of hydration water molecules (same as reported in Figure 1-B), compared to the theoretical difference spectra calculated for each of the two interfacial H-Bond populations, HB-wrap (orange) and Hydration2bulk (blue), for 0.5 M concentration and temperature of 290 K. The statistical error associated to the theoretical spectral calculation, estimated as described here in the SI, is also reported. Bottom: Theoretical difference spectra for the two HB-populations (same as top panel and Figure 1-B) now reported without the error bars.*

The signals arising from the HB-wrap and Hydration2bulk populations are obtained with the following procedure. Firstly, the water molecules belonging to the inner/outer layers, i.e. being located at a distance from the solute vdW surface smaller/greater than 2 Å, are selected at each MD-

step. Once this is done, the correlation function in Eq.11 (for the total spectrum of the whole system) can be rewritten as follows:

$$I(\omega) = \frac{2\pi\beta}{3cV} \sum_{u=x,y,z} \left(\sum_{m=1}^{3N_{inner}} \sum_{l=1}^{3N} \int_{-\infty}^{+\infty} dt\, e^{i\omega t} \langle P_{um}(t) v_m(t) P_{ul}(0) v_l(0) \rangle + \sum_{m=1}^{3N_{rest}} \sum_{l=1}^{3N} \int_{-\infty}^{+\infty} dt\, e^{i\omega t} \langle P_{um}(t) v_m(t) P_{ul}(0) v_l(0) \rangle \right)$$

(13)

where N_{inner} identifies all water molecules in the inner layer and N_{rest} all the remaining water molecules in the simulation box, i.e. the ones in the outer layer (N_{outer}) + the ones that are located outside the hydration layer in the bulk (N_{bulk}). Note that $N = N_{inner} + N_{outer} + N_{bulk}$.

The 1st term in Eq.13 can be further decomposed by partitioning the sum l=1,N into $l=1,N_{inner}$ + $l=1,N_{rest}$, so that:

$$\sum_{m=1}^{3N_{inner}} \sum_{l=1}^{3N} \int_{-\infty}^{+\infty} dt\, e^{i\omega t} \langle P_{um}(t) v_m(t) P_{ul}(0) v_l(0) \rangle \quad (14)$$

$$= \sum_{m=1}^{3N_{inner}} \left(\sum_{l=1}^{3N_{inner}} \int_{-\infty}^{+\infty} dt\, e^{i\omega t} \langle P_{um}(t) v_m(t) P_{ul}(0) v_l(0) \rangle + \sum_{l=1}^{3N_{rest}} \int_{-\infty}^{+\infty} dt\, e^{i\omega t} \langle P_{um}(t) v_m(t) P_{ul}(0) v_l(0) \rangle \right) = FFT[\langle inner\ inner \rangle + \langle inner\ rest \rangle]$$

where FFt stands for the Fourier transform. In Eq.14, the first part $\langle inner\ inner \rangle$ only includes the cross correlation terms in between water molecules belonging to the inner layer. In the 100-210 cm^{-1} frequency range, such cross correlation terms provide the intermolecular stretching mode of the HBs formed in between water molecules in the inner layer, i.e. of the HB-wrap population.

The second part $\langle inner\ rest \rangle$ includes the cross correlation terms in between water in the inner layer and all other water molecules , hence giving the intermolecular stretching mode of the HBs formed in between water molecules in the inner layer and all other water molecules, which are part of the HB-Hydration2bulk population.

Also the second term in Eq.13 can be decomposed into the contribution from H-Bonds that are of the HB-Hydration2bulk kind, and the contribution from H-Bonds formed in between bulk water molecules, by partitioning the sum m=1,N_{rest} into m=1,N_{outer} + m=1,N_{bulk} and the sum l=1,N into l=1,N_{inner} + l=1,N_{outer} + l=1,N_{bulk} :

$$\sum_{m=1}^{3N_{rest}} \sum_{l=1}^{3N} \int_{-\infty}^{+\infty} dt\, e^{i\omega t} \langle P_{um}(t) v_m(t) P_{ul}(0) v_l(0) \rangle \qquad (15)$$

$$= FFT[\langle outer\ inner \rangle + \langle outer\ outer \rangle + \langle outer\ bulk \rangle + \langle bulk\ inner \rangle + \langle bulk\ outer \rangle + \langle bulk\ bulk \rangle]$$

Among all these terms, only the ones related to HBs of the HB-hydration2bulk type (like $\langle outer\ inner \rangle\ and\ \langle bulk\ inner \rangle$), i.e. connecting the wrap to the bulk, will be relevant in the difference spectra.

The lifetime of the two HB-populations is estimated from the MD simulations by evaluating the water-water H-bond autocorrelation function ($C_{HB}(t)$):

$$C_{HB}(t) = \langle \frac{h(0)h(t)}{h(0)h(0)} \rangle$$

where the operator h(t) gives one, if a given H-Bond is intact at time t and 0 otherwise. Note that the same criterion as for all the other HB analysis has been adopted.

From the above correlation function, the HB-lifetime (τ_{HB}) is defined as the time required for $C_{HB}(t)$ to decay to 1/e. The resulting τ_{HB} values are equal to 1.36 ps and 1.08 ps for HB-wrap and HB-hydration2bulk respectively (to be compared to the value of 1.04 ps obtained for bulk water). The longer lifetime for the HBs formed within the inner layer (i.e. HB-wrap) than for the Hydration2bulk population nicely correlate with the decrease in hydration entropy discussed in the manuscript, i.e. a higher hydration entropy cost associated with the water molecules in the inner layer than with the ones in the outer layer.

The vibrational period of the THz investigated modes (T=1/(ν_0)) is directly related frequency. The vibrational period is 0.20 ps and 0.17 ps for the164 and 195 cm^{-1} hydration water bands, respectively. This implies that the lifetime of each hydrogen bond is 5 times longer than the vibrational period. This is in line with the experimental observation of a damped harmonic vibration. However, we want to add that whereas single hydrogen bonds can be broken, the hydration bond motif remains intact over a much longer period, it persists longer than our simulation time, i.e. 100 ns.

Figure S6 shows how HB-wrap and Hydration2bulk populations have well defined separate contributions in the 120-240 cm^{-1} domain at the two temperatures presented here, which maxima correspond to the maxima of the two positive components of the experimental fit (orange and blue curves): The 161 cm^{-1} lower frequency part of the 184 cm^{-1} band (in the total difference spectra, Figure 1-A of the main text) is due to the HB-wrap population, while the 193 cm^{-1} higher frequency part is due to the Hydration2bulk population. The theoretical difference spectra calculated for HB-wrap and Hydration2bulk are also shown in the figure to have the same temperature dependence for the two positive components of the experimental fit: the intensity of Hydration2bulk band (blue) strongly decreases with temperature, becoming almost zero at 310 K, while the HB-wrap band is clearly observed also at the high temperature. The persistence of the 164 cm^{-1} band is the spectroscopic marker of the 2D-H-bond network in the hydration shell maintained also at high temperatures and high concentrations (see also Figure 1 in the Main Text, Figure S6, Table S1 and Ref.[14]).

We now evaluate in Figure S6-B the effect of statistical errors in the theoretical and experimental THz spectra calculations on the theory-experiment comparison presented in the Figure 1-B of the main text. Error bars have been obtained for the theoretical spectra in the following way. We calculated these spectra separately for both halves of the trajectory. The errors due to limited sampling time are hence displayed in the figure by evaluating the minimum and maximum intensity values for each frequency. Experimentally our statistical error is smaller than the size of the line in the figure. Thus, the center frequency for both hydration water bands agree very well within their statistical error when we compare experiment and simulations.

Tert-Butanol signatures in the THz spectra

As shown in Figure S7, the solute contributes to the THz-IR spectrum of aqueous *tert*-butanol at both 290 K and 310 K temperatures, however these *tert*-butanol spectral contributions are negligible in the 0-200 cm^{-1} region. Above 200 cm^{-1}, the solute contribution is significant, thus we restricted our comparison of the experimental and theoretical spectrum to the frequency range below 250 cm^{-1}.

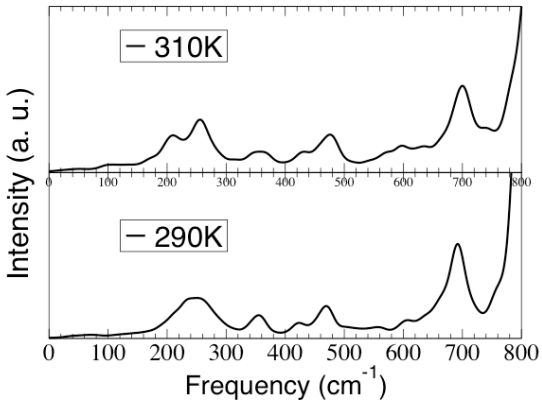

Figure S7: Theoretical THz-IR spectra. *Theoretical THz-IR spectra calculated from DFT-MD simulations at 290 K and 310 K, using Eq.11 and including the contribution of tert-butanol atoms only.*

Orientational and translational water dynamics in the hydration layer

In Figure S8 we evaluate the orientational and translational dynamics of water in the inner and outer hydration layers around *tert*-butanol at a temperature of 293 K.

As regards the orientation dynamics, we have calculated the orientational correlation function of the dipole vector of the water molecules as:

$$C_{\mu}^{(l)}(t) = \frac{\langle P_l(e^{\mu}(t)e^{\mu}(0))\rangle}{\langle P_l(e^{\mu}(0)e^{\mu}(0))\rangle} \qquad (17)$$

where P^l is the l-th rank Legendre polynomial and $e^{\mu}(t)$ is the water dipole moment (unit vector) at time t. The orientation relaxation time, $\tau_{\mu}^{(l)}$, is given by the time integral

$$\tau_{\mu}^{(l)} = \int_0^{\infty} C_{\mu}^{(l)}(t)\, dt, \qquad (18)$$

l = 2 is used. [36-38]

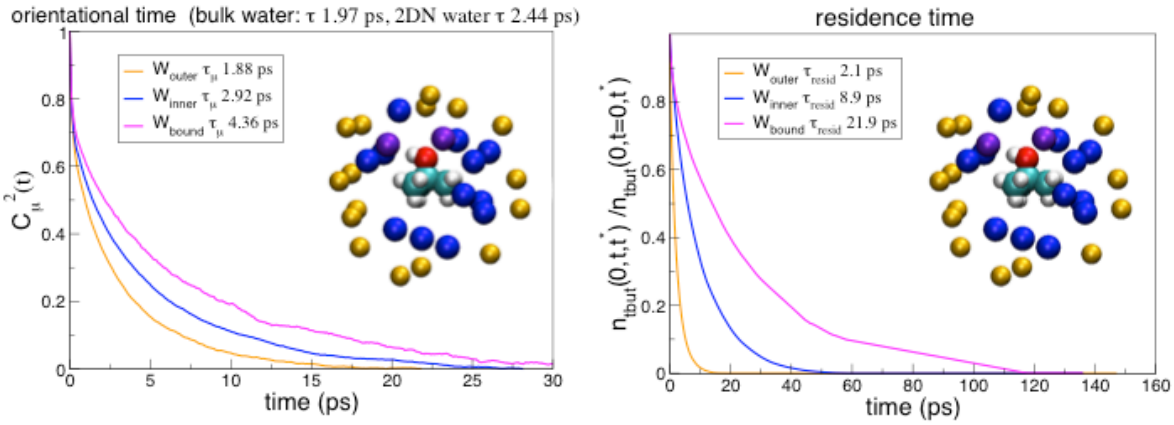

Figure S8: Correlation functions for orientational and translational hydration water dynamics. *Orientation (left) and residence (right) times calculated from a classical MD simulation of hydrated tert-butanol at 293 K for: water in the outer hydration layer (W_{outer}, orange), water forming the HB-wrap in the inner layer (W_{inner}, blue) and water in the inner layer which is also H-Bonded to the alcohol OH group (W_{bound}, violet). In the case snapshots, the molecules in the hydration layer are colored according to the population they belong to. The reference orientation time values for water in the bulk and water forming the 2D-HB-Network at the air-water interface are taken from Ref.*[36]

The residence time of water in the inner/outer layer have been calculated using the formalism introduced by Impet et al. in Ref.[39] We define a function $P_j(t0,t,t^*)$ which is a property of the j-th water molecule. It is equal to 1 if the j-th water is part of the selected (inner/outer) layer from time t0 to t, without leaving the layer for periods longer than t^*, and it is equal to 0 otherwise. We can thus define the average quantity $n_{tbut}(t)$, property of the *tert*-butanol solute, as:

$$n_{tbut}(to,t,t^*) = \sum_{j=1}^{N_{hyd}(t0)} P_j\ (to,t,t^*) \qquad (19)$$

where the sum run over all the hydration water molecules that at time t0 belong to the selected (inner/outer) layer. The parameter t^* is introduced to take account of water molecules which leave the layer only temporarily and return to it without ever having properly entered another layer. The value t^*=0.5 ps has been optimized by observing the timescales during the simulation for water that exit and re-enter the inner/outer layers. Any other value for t^* in the range 0-2 ps provides the same ratio among the residence times of water in the inner and outer layers as well as H-Bonded to the alcohol OH function.

Both orientation and residence times have been calculated form the classical MD simulations separately for water forming the HB-wrap in the inner layer (denoted W_{inner}) and water in outer layer (denoted W_{outer}), as identified at each MD step through the ten descriptors described in the main text and summarized in Table 1. We have further distinguished within the inner layer the water molecules that on top of being part of the HB-wrap are also H-Bonded to the alcohol OH-group (denoted W_{bound}).

Hydrophobic solvation entropy is related to cavity formation

Cavity formation play a major role, and we also find that it provides the largest contribution to hydration entropy, as also shown in Ref. 14. In order to quantify this effect, we have now plotted all contributions to hydration entropy in Figure S9. The total hydration entropy $\Delta S_{TOT}(T)$ can be exactly rewritten as the contribution due to cavity formation $\Delta S_{cavity}(T)$ plus the remaining hydration water entropy contribution ΔS^*, arising from the different structure assumed by water in the hydration layer with respect to bulk. Within our THz-calorimetry approach (fully detailed here in the SI and in Ref. 14), $\Delta S_{cavity}(T)$ is estimated from THz-spectra at 400 K. At 400 K, the Hydration2bulk population is decreased to zero, Thus, at 400 K we are left only with a contribution ($\Delta S_{solv}(400)$) due to cavity formation. Knowing this, the contribution due to cavity formation at any other temperature can be obtained as $\Delta S_{cavity}(T) = \Delta S_{solv}(400) + \Delta C_P\ (400)\ \log(T/T_{ref}=400\ K)$, where both $\Delta S_{solv}(400)$ and $\Delta C_P\ (400)$ values have been deduced before (Ref. 14). ΔS^* is then given by $\Delta S = \Delta S_{TOT} - \Delta S_{cavity}$.

As can be seen in the figure below, ΔS_{cavity} provides the largest contribution to hydration entropy, showing that our findings fully reconcile with the results previously obtained by Chandler and coworkers[40].

What we can also notice is that ΔS_{cavity} decreases by 20% in going from T=273 K (where ΔS_{cavity}=-74.4 J mol^{-1} K^{-1}) to T=313 K (where ΔS_{cavity}=-59.2 J mol^{-1} K^{-1}), while ΔS^* decreases by 70% (ΔS^*=-29.0 J mol^{-1} K^{-1}at T=273 K and ΔS^*=-9.0 J mol^{-1} K^{-1}at T=313 K).

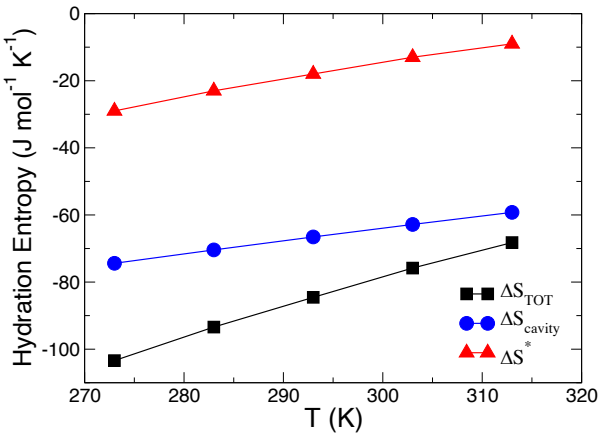

Figure S9. THz calorimetry. *Comparison of the experimentally determined (with THz-calorimetry) hydration entropy* ΔS_{TOT} *with the contribution related to cavity formation* $\Delta S_{cavity} = \Delta S_{solv}(400) + \Delta C_P\ (400)\ \log(T/T_{ref}=400\ K)$*, and the remaining hydration water entropy contribution* ΔS^* *(as defined in the main text). Note that* $\Delta S_{TOT} = \Delta S^* + \Delta S_{cavity}$.

REFERENCES

1. Hess B, Kutzner C, van der Spoel D, Lindahl E (2008) GROMACS 4: Algorithms for Highly Efficient, Load-Balanced, and Scalable Molecular Simulation. *J. Chem. Theory Comput.* 4: 435–447.

2. Jorgensen WL, Maxwell DS, Tirado-Rives J (1996) Development and Testing of the OPLS All-Atom Force Field on Conformational Energetics and Properties of Organic Liquids. *J. Am. Chem. Soc.* 118: 11225-11236.

3. Abascal JLF, Vega C (2005) A general purpose model for the condensed phases of water: TIP4P/2005. *J. Chem. Phys.* 123: 234505.

4. Darden T, York D, Pederson L (1993) Particle mesh Ewald: An N log(N) method for Ewald sums in large systems. *J. Chem. Phys.* 98:10089–10092.

5. Essmann U, Perera L, Berkowitz ML (1995) A smooth particle mesh Ewald method. *J. Chem. Phys.* 103: 8577–8592.

6. Miyamoto S, Kollman PA (1992) Settle: An analytical version of the SHAKE and RATTLE algorithm for rigid water models. *J. Comp. Chem.* 13: 952–962.

7. Bussi G, Donandio D, Parrinello M (2007) Canonical sampling through velocity rescaling. *J. Chem. Phys.* 126: 014101.

8. Berendsen HJC et al. (1984) Molecular dynamics with coupling to an external bath. *J. Chem. Phys.* 81: 3684–3690.

9. Nosé S (1984) A unified formulation of the constant temperature molecular dynamics methods. *Mol. Phys.* 52: 255–268.

10. Hoover WA (1985) Canonical dynamics: Equilibrium phase-space distributions. *Phys. Rev. A* 31: 1695–1697.

11. Errington JR, Debenedetti PG (2001) Relationship between structural order and the anomalies of liquid water. *Nature* 409: 318–321.

12. Persson RAX, Pattni V, Singh A, Kast M, Heyden M (2017) Signatures of Solvation Thermodynamics in Spectra of Intermolecular Vibrations. *J. Chem. Theory Comput.* 13: 4467−4481.

13. Lin S-T, Maiti PK, Goddard III WA (2010) Two-Phase Thermodynamic Model for Efficient and Accurate Absolute Entropy of Water from Molecular Dynamics Simulations. *J. Phys. Chem. B* 114: 8191-8198.

14. Böhm F, Schwaab G, Havenith M (2017) Mapping Hydration Water around Alcohol Chains by THz Calorimetry. *Angew. Chem. Int. Ed.* 56: 9981–9985.

15. Schwaab G, Sebastiani F, Havenith M (2019) Ion hydration and ion pairing as probed by THz spectroscopy. *Angew. Chem. Int. Ed.* 58: 3000–3013

16. Bowron DT, Finney JL, Soper AK (1998) Structural investigation of solute-solute interactions in aqueous solutions of tertiary butanol. *J. Phys. Chem. B*, 102: 3551-3563.

17. Nishikawa K, Kodera Y, Iijima T (1987) Fluctuations in the particle number and concentration and the Kirkwood-Buff parameters of tert-Butyl alcohol and water mixtures studied by Small-Angle X-ray Scattering. *J. Phys. Chem.* 91: 3694-3699.

18. Overduin D, Patey GN (2017) Comparison of simulation and experimental results for a model aqueous tert-butanol solutions. *J. Chem. Phys.* 147: 024503.

19. Kežić B, Perera A (2012) Aqueous tert-butanol mixtures: A model for molecular-emulsions. *J. Chem. Phys.* 137: 014501.

20. Rankin M, Ben-Amotz D, van der Post ST, Bakker HJ. (2015) Contacts between alcohols in water are random rather than hydrophobic. *J. Phys. Chem. Lett.* 6: 688−692.

21. Wilcox DS, Rankin BM, Ben-Amotz D (2013) Distinguishing aggregation from random mixing in aqueous *t-butyl* alcohol solutions. *Faraday Discuss.* 167: 177-190.

22. Hutter J, Iannuzzi M, Schiffmann F, & VandeVondele J (2014) CP2K: Atomistic Simulations of Condensed Matter Systems. *WIREs Comput. Mol. Sci.* 4: 15−25.

23. VandeVondele J, Krack M, Mohamed F, Parrinello M, Chassaing T, Hutter J (2005) Quickstep: Fast and Accurate Density Functional Calculations Using a Mixed Gaussian and Plane Waves Approach. *Comput. Phys. Commun.* 167: 103−128.

24. Becke AD (1988) Density-Functional Exchange-Energy Approximation with Correct Asymptotic Behavior. *Phys. Rev. A: At., Mol., Opt. Phys.* 38: 3098−3100.

25. Lee C, Yang W, Parr RG (1988) Development of the Colle-Salvetti Correlation-Energy Formula into a Functional of the Electron Density. *Phys. Rev. B: Condens. Matter Mater. Phys.* 37: 785−789.

26. Grimme S (2006) Accurate Description of van der Waals Complexes by Density Functional Theory Including Empirical Corrections. *J. Comput. Chem.* 25: 1463−1473.

27. Grimme S (2006) Semiempirical GGA-Type Density Functional Constructed with a Long-Range Dispersion Correction. *J. Comput. Chem.* 27: 1787−1799.

28. Goedecker S, Teter M, Hutter J (1996) Separable Dual-Space Gaussian Pseudopotentials. *Phys. Rev. B: Condens. Matter Mater. Phys.* 54: 1703−1710.

29. Pezzotti S, Galimberti DR, Gaigeot MP (2017) 2D H-Bond Network as the Topmost Skin to the Air–Water Interface. *J. Phys. Chem. Lett.* 8: 3133-3141.

30. Galimberti DR, Milani A, Tommasini M, Castiglioni C, Gaigeot MP (2017) Combining static and dynamical approaches for infrared spectra calculations of gas phase molecules and clusters. *J. Chem. Theory and Comp.*13: 3802-3813.

31. Galimberti D, Milani A, Castiglioni C (2013) Infrared intensities and charge mobility in hydrogen bonded complexes. *J. Chem. Phys.* 139: 074304.

32. Torii H (2017) Dynamical behavior of molecular partial charges implied by the far-infrared spectral profile of liquid water. *Chem. Phys.* 512: 165-170.

33. Frisch MJ, *et al*. (2016) Gaussian 09, Gaussian, Inc., Wallingford CT.

34. White JA, Schwegler E, Galli G, Gygi F (2000) The solvation of Na+ in water: First-principles simulations. *J. Chem. Phys.* 113: 4668–4673.

35. Grechko MS, *et al.* (2018) Coupling between intra- and intermolecular motions in liquid water revealed by two-dimensional terahertz-infrared-visible spectroscopy. *Nat. Comm.* 9: 885.

36. Pezzotti S, Serva A, Gaigeot MP (2018) 2D-HB-Network at the air-water interface: a structural and dynamical characterization by means of ab-initio and classical molecular dynamics simulations. *J. Chem. Phys.* 148: 174701.

37. Luzar A (2000) Resolving the hydrogen bond dynamics conundrum. *J. Chem. Phys.* 113: 10663–10675.

38. Chandra A (2003) Dynamical behavior of anion-water and water-water hydrogen bonds in aqueous electrolyte solutions: A molecular dynamics study. *J. Phys. Chem. B* 107: 3899–3906.

39. Impey RW, Madden PA, McDonald IR (1983) Hydration and Mobility of Ions in Solution. *J. Phys. Chem.* 87: 5071-5083.

40. Lum K, Chandler D, Weeks JD (1999) Hydrophobicity at small and large length scales. *J. Phys. Chem. B* 103: 4570-4577.